

ABCA4 Variant c.5714+5G>A in *Trans* With Null Alleles Results in Primary RPE Damage

Jana Sajovic,^{1,2} Andrej Meglič,¹ Zelia Corradi,^{3,4} Mubeen Khan,³⁻⁵ Aleš Maver,⁶ Martina Jarc Vidmar,^{1,2} Marko Hawlina,^{1,2} Frans P. M. Cremers,^{3,4} and Ana Fakin^{1,2}

¹Eye Hospital, University Medical Centre Ljubljana, Ljubljana, Slovenia

²Faculty of Medicine, University of Ljubljana, Ljubljana, Slovenia

³Department of Human Genetics, Radboud University Medical Center, Nijmegen, the Netherlands

⁴Donders Institute for Brain, Cognition and Behaviour, Radboud University, Nijmegen, the Netherlands

⁵Max Planck Institute for Psycholinguistics, Nijmegen, the Netherlands

⁶Clinical Institute of Genomic Medicine, University Medical Centre Ljubljana, Ljubljana, Slovenia

Correspondence: Ana Fakin, Eye Hospital, University Medical Centre Ljubljana, Ljubljana, Slovenia, Grablovičeva ulica 46, Ljubljana 1000, Slovenia; ana.fakin@kclj.si

Received: February 28, 2023

Accepted: August 30, 2023

Published: September 20, 2023

Citation: Sajovic J, Meglič A, Corradi Z, et al. *ABCA4* variant

c.5714+5G>A in *trans* with null alleles results in primary RPE damage. *Invest Ophthalmol Vis Sci.* 2023;64(12):33.

<https://doi.org/10.1167/iovs.64.12.33>

PURPOSE. To determine the disease pathogenesis associated with the frequent *ABCA4* variant c.5714+5G>A (p.[=,Glu1863Leufs*33]).

METHODS. Patient-derived photoreceptor precursor cells were generated to analyze the effect of c.5714+5G>A on splicing and perform a quantitative analysis of c.5714+5G>A products. Patients with c.5714+5G>A in *trans* with a null allele (i.e., c.5714+5G>A patients; $n = 7$) were compared with patients with two null alleles (i.e., double null patients; $n = 11$); with a special attention to the degree of RPE atrophy (area of definitely decreased autofluorescence and the degree of photoreceptor impairment (outer nuclear layer thickness and pattern electroretinography amplitude)).

RESULTS. RT-PCR of mRNA from patient-derived photoreceptor precursor cells showed exon 40 and exon 39/40 deletion products, as well as the normal transcript. Quantification of products showed 52.4% normal and 47.6% mutant *ABCA4* mRNA. Clinically, c.5714+5G>A patients displayed significantly better structural and functional preservation of photoreceptors (thicker outer nuclear layer, presence of tubulations, higher pattern electroretinography amplitude) than double null patients with similar degrees of RPE loss, whereas double null patients exhibited signs of extensive photoreceptor damage even in the areas with preserved RPE.

CONCLUSIONS. The prototypical STGD1 sequence of events of primary RPE and secondary photoreceptor damage is congruous with c.5714+5G>A, but not the double null genotype, which implies different and genotype-dependent disease mechanisms. We hypothesize that the relative photoreceptor sparing in c.5714+5G>A patients results from the remaining function of the *ABCA4* transporter originating from the normally spliced product, possibly by decreasing the direct bisretinoid toxicity on photoreceptor membranes.

Keywords: STGD1, c.5714+5G>A, splicing, PERG, autofluorescence

Stargardt disease (STGD1), also known as *ABCA4* retinopathy, is the most frequent retinal dystrophy caused by a single gene, affecting approximately 1 in 8000 to 10,000 people.¹ The *ABCA4* protein, encoded by the *ABCA4* gene, is situated in rod and cone photoreceptor outer segment disks and lamellae, respectively²⁻⁵ and functions as a transmembrane transporter of molecules involved in the visual transduction.^{6,7} Despite this progress and improvements in our understanding of STGD1, the pathogenesis is still poorly understood, which is precluding the development of treatment strategies.

STGD1 is known for a very heterogeneous phenotypic appearance,⁸⁻¹⁰ which is reflected in numerous clinical classifications, such as categorization according to fundus appearance (Fishman classification),¹¹ electroretinography (ERG),¹² presence or absence of foveal atrophy,^{8,9,13-18} and age at onset.¹⁵

With the widespread availability of genetic diagnosis, attempts are being made to connect the clinical variability with the nature of the causative alleles.^{8,9,13,14,19-22} Patients with two null alleles have been shown to have the most severe disease, that is, childhood onset cone-rod dystrophy.¹³

Characterization of other, non-null alleles has been more challenging^{8,23} because there are >2000 disease-associated variants (www.lovd.nl/ABCA4, accessed May 8, 2023) that, owing to the recessive nature of disease, combine in thousands of different pairings. Characterisation of *ABCA4* variants is further complicated owing to limitations in performing functional assays.

Retinal tissue of living patients is not readily available and *ABCA4* gene expression in accessible somatic cells is very low²⁴⁻²⁶; therefore, other approaches, such as in vitro assays or patient-derived photoreceptor precursor cells



(PPCs) need to be used to study the effect of different variants.^{27–29}

The noncanonical splice site variant c.5714+5G>A (p.[=,Glu1863Leufs*33]), located in the 5' splice region of intron 40,³⁰ is the sixth most frequent variant in patients with STGD1,³¹ identified in 1% to 16% of cases^{9,32–35} and recurrent in Newfoundland cases owing to a major founder effect.³⁶ Despite that, the effect of c.5714+5G>A variant on structural and functional retinal changes has not yet been systematically addressed.

In the Slovenian registry of patients with *ABCA4* retinopathy, c.5714+5G>A is the fourth most frequent variant, present in 12% of patients, which provides an opportunity to perform a detailed phenotypic specification. Moreover, an ex vivo assay using PPC has been developed at the Radboudumc Stem Cell Technology Center in the Netherlands to study the variant's effect in conditions most closely resembling in vivo situation. Combining the two approaches, this study provides insights into disease pathogenesis associated with one of the most frequent *ABCA4* variants.

METHODS

Ethics and Declarations

This study was conducted according to the tenets of the Declaration of Helsinki. The procedures for obtaining human blood samples for ex vivo part were approved by the local Ethical Committee in Nijmegen (protocol ID number: 2018–4516). The clinical part was reviewed and approved by the National Medical Ethics Committee of the Republic of Slovenia (protocol ID number: 0120-50/2021/3). Written informed consent was obtained from participants before their enrollment.

Ex Vivo Analysis

Epstein–Barr Virus (EBV) Transformation of Human Blood. Blood was collected from one control individual and an individual with STGD1 carrying the *ABCA4* variants c.5714+5G>A; p.[=,Glu1863Leufs*33] and c.4539+1G>T; p.(?). Stable lymphoblastoid cell lines were obtained from the peripheral blood of the control and STGD1 individual by EBV transformation following the previously described protocol.³⁷ Briefly, white blood cells were isolated from blood samples and resuspended in EBV supernatant. After 2 hours of incubation, cells were pelleted, resuspended with cyclosporine solution, and placed to grow in 24-well plates in a 37°C and 7.5% CO₂ incubator. After 2 weeks, the cultures were assessed with a microscope.

Generation of Induced Pluripotent Stem Cells and Differentiation Into Photoreceptor Precursor Cells. EBV immortalized lymphoblasts were cultured in mononuclear cell medium for 5 days in a T75 flask. Subsequently, reprogramming into induced pluripotent stem cells was performed following a previously described method. In short, four lentiviral vectors containing the pluripotency genes OCT3/4, NANOG, *KLF4*, and c-MYC were used for the transduction of EBV lymphoblasts. The cells were then cultured on growth factor-reduced Matrigel (Corning Life Sciences, Tewksbury, MA, USA) in Essential 8 Flex medium (Thermo Fisher Scientific, Waltham, MA, USA) and passaged as clumps at a ratio of 1:5 to 1:10 every 5 to 6 days by digestion with 0.5 mM EDTA. Cells were maintained at 37°C and 5% CO₂. At passage 10, immunocytochemistry and

quantitative RT-PCR were performed to characterize induced pluripotent stem cells and assess pluripotency markers as described in the protocol (see Supplementary Figs. S1, S2, and S3).³⁸

For differentiation, the Flamier et al.³⁹ protocol was followed. DMEM/F12 medium was supplemented with non-essential amino acids (NEAA; Sigma-Aldrich, St. Louis, MO, USA), N2 supplements (Thermo Fisher Scientific), B27 supplements (Thermo Fisher Scientific), heparin (Sigma-Aldrich), insulin-like growth factor-1 (Sigma-Aldrich), recombinant basic FGF (STEMCELL Technologies, Vancouver, Canada), and human recombinant COCO (R&D Systems, Inc., Minneapolis, MN, USA). The cells were characterized after 1 month of differentiation, during which the medium was changed daily.

Induced Pluripotent Stem Cells and Photoreceptor Precursor Cells Characterization. The characterization of the patient and control lines was performed by comparing expression of differentiation markers between induced pluripotent stem cells and PPCs by quantitative PCR (see Supplementary Fig. S4). RNA was isolated from collected cells using the NucleoSpin RNA Clean-up Kit (Macherey-Nagel, Duren, Germany) and cDNA was synthesized with the iScript cDNA synthesis kit (Bio-Rad Laboratories, Hercules, CA, USA) starting from 1 µg of RNA. For both experiments the manufacturer's protocol were followed.

Quantitative PCR was performed using GoTaq Real-Time quantitative PCR Master Kit (Promega, Madison, WI, USA). The primers for the selected differentiation markers and the housekeeping gene *GUSB* are reported in Supplementary Table S1. Each reaction was set up in triplicate and performed in technical duplicate using the 7900HT fast real-time PCR system. The 2^{-(ΔΔCt)} method was used to assess the relative expression of the markers, values are reported as the average with SD of the technical duplicates.

***ABCA4* Transcript Analysis.** For *ABCA4* transcript analysis, PPCs derived from the healthy individual and the STGD1 proband were harvested after 30 days of differentiation. Cells were treated with cycloheximide (CHX; Sigma-Aldrich) 24 hours before collection to suppress nonsense-mediated decay. RNA isolation and cDNA synthesis were performed as described above.

RT-PCR analysis was performed using primers located in exon 38 (forward) and exon 44 (reverse) of *ABCA4*. The following conditions were used to perform RT-PCR: 94°C for 2 minutes, 35 cycles of 30 seconds at 94°C, 30 seconds at 58°C, 90 seconds at 72°C, and a final elongation of 2 minutes at 72°C. Actin Beta (*ACTB*) was used as house-keeping gene.

RT-PCR products were resolved on 2% agarose gel, purified using the Nucleospin Gel and PCR Clean-up Kit (Macherey-Nagel, Duren, Germany) and analyzed by Sanger sequencing. Fiji software⁴⁰ was used to perform semi-quantification of the ratio between different transcripts. Semi-quantification was done in a technical duplicate (see Supplementary Table S2) on the most representative biological.

Clinical Analysis

Patients. The study included 18 patients with a clinical and molecular diagnosis of STGD1, recruited from the STGD1 cohort overseen at the Eye Hospital, University Medical Centre Ljubljana based on their genotype. The main study group (c.5714+5G>A patients; *n* = 7; 4 males), were

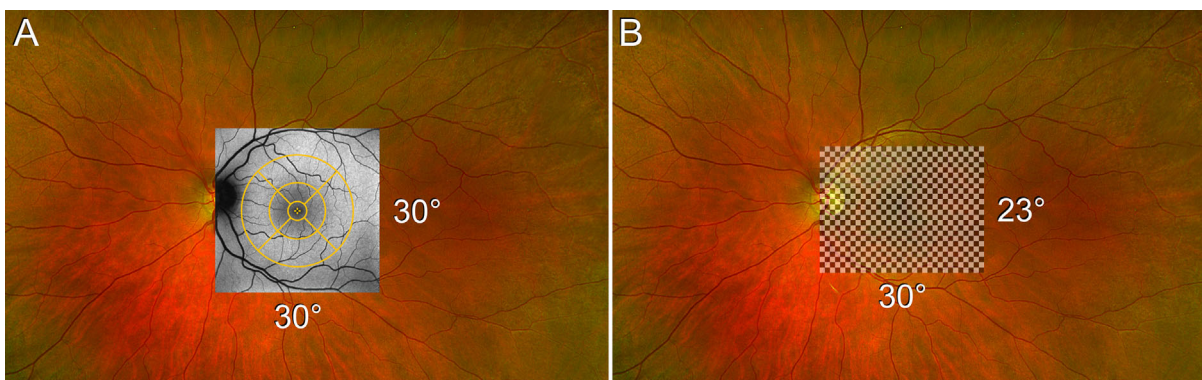


FIGURE 1. Analyzed retinal area. Schematic representation of the area of the retina imaged using 30° FAF imaging (for assessing RPE damage) and SD-OCT (for assessing photoreceptor damage) (A) and stimulated when performing PERG (for assessing photoreceptor function) (B).

patients with the splicing variant c.5714+5G>A in *trans* with a null variant, which allowed us to study this variant in isolation. The control group were patients with two null variants (double null patients; $n = 11$; 3 males). For the purpose of this study, a variant was considered to be null if it was either a stop variant, a frame-shifting variant resulting in a stop codon, or splicing and missense variants previously shown to behave as null.¹⁵ The specific patients' variants are listed in Supplementary Table S3. In a group of patients with c.5714+5G>A allele, there were five unrelated patients and one sibling pair, whereas the group of double null patients consisted of seven unrelated patients and two sibling pairs.

Clinical Evaluation. Clinical evaluation included age at onset (age when patients noted loss of visual acuity), disease duration (difference between the age at examination and age of onset), best-corrected visual acuity (BCVA), ERG (Diagnosys LLC, Littleton, MA, USA; recorded according to the standards of the International Society of Clinical Electrophysiology of Vision^{41,42}; fundus autofluorescence (FAF) and SD-OCT (Heidelberg Engineering, Heidelberg, Germany). A similar retinal area of approximately 30° × 30° was analyzed with FAF, OCT, and pattern ERG (PERG), allowing a comparison between the parameters describing impairment of RPE and photoreceptors (Fig. 1). In a subgroup of patients ($n = 14$), fixation and retinal sensitivity to light were evaluated in mesopic conditions with a Nidek MP1 microperimetry (Nidek Technologies, Padova, Italy).

BCVA was measured using Snellen charts and transformed to the logMAR equivalent. A threshold of ≥ 1.0 logMAR was chosen to represent legal blindness. Kaplan–Meier survival analysis was performed using BCVA on the eye with a better VA. The area of definitely decreased autofluorescence (DDAF) was measured on FAF to represent the degree of RPE loss; the thickness of the outer nuclear layer (ONL) was measured on OCT to represent the degree of photoreceptor loss, and PERG amplitude was used to represent the degree of photoreceptor dysfunction in the macula. Additionally, full-field ERG amplitudes, reflecting peripheral retinal function, were evaluated and compared between the two groups. For the DDAF and ONL analyses, patients were masked to the graders. Detailed description on ERG, FAF, OCT, and microperimetry analyses are provided in the Supplementary Materials and Methods.

Genetic Analysis. Peripheral venous blood samples were obtained and genomic DNA was extracted from blood samples according to the standard procedure. Sequencing of

the *ABCA4* gene in 13 patients was performed using Illumina Nextera Coding Exome capture protocol, with subsequent sequencing on Illumina NextSeq550 (Illumina, San Diego, CA, USA). In three patients, sequencing of the entire *ABCA4* genomic locus was performed using single molecule molecular inversion probes library preparation and the Illumina NextSeq500 sequencing platform.⁴³ The variants' segregation with the disease in available families was analyzed by Sanger sequencing. In addition, Sanger sequencing was performed to confirm identified variants in two siblings.

Statistical Analyses. Data were analyzed using IBM SPSS Statistics software version 27.0 (IBM Corp. Armonk, NY, USA). The Mann–Whitney U test was used to compare median values of the measured parameters between the two patient groups, followed by multiple linear regression to account for the effect of age. Simple linear regression was used to study the effect of age on DDAF, PERG, and ONL, with age as the independent variable, whereas DDAF, PERG, and ONL were taken as dependent variables. A Spearman rank correlation test was adopted to assess whether there was a correlation between the degree of RPE atrophy (represented by the DDAF area) and loss of photoreceptors (represented by ONL thickness and PERG P50 amplitudes) within each genotype group. This process was followed by a multiple linear regression to explore genotype differences between ONL thickness and PERG P50 amplitudes for the same DDAF area. A Kaplan–Meier survival curve was used to determine the age when 50% of patients reached legal blindness. For this analysis, 4 of the 11 double null patients were excluded, because it was not possible to reliably determine the time when their BCVA decreased to ≥ 1.0 logMAR owing to a lack of BCVA data at early stages. Log-rank testing was used to test for statistical differences between the survival curves of the two patient groups. A P value of <0.05 was considered to indicate statistical significance.

For the comparison of median values between the two groups, the measurements around the time of the last ERG examination were used, because the ERG is performed least frequently owing to a high level of difficulty and time consumption and most other examinations were available at a similar time point. For correlations, examinations were considered to have been performed at a similar time point if done within 2 years of ERG testing. For one c.5714+5G>A patient, we excluded OCT data for this analysis because they were not performed within the 2 years from ERG examination. Longitudinal analysis of the DDAF area, ONL thickness,

and PERG P50 amplitude was performed with all available data. There was good interocular symmetry in all patients and the right eye was used to compare the structural and functional parameters between the two groups.

Data Availability

The data that support the findings of this study are available on request from the corresponding author A.F. or the first author J.S. The data are not publicly available because they contain information that could compromise research participant privacy.

RESULTS

Ex Vivo Analysis: *ABCA4* Variant c.5714+5G>A Results in Partial Exon Skipping Retaining Approximately One-Half of Normally Spliced mRNA

To determine the effect of variant c.5714+5G>A on splicing in a retina-specific context, PPCs were generated from a STGD1 patient carrying c.5714+5G>A in *trans* with variant c.4539+1G>T. Variant c.4539+1G>T was thought to behave as null owing to its homozygous presence in persons with panretinal dystrophy.³⁰ Moreover, two noncanonical splice site variants affecting the same splice donor site, c.4538A>G and c.4538A>C, when analyzed in vitro in human embryonic kidney (HEK293T) cells using midigenes, resulted in a 30-nt elongation of exon 30 and the skipping of exon 30, yielding the RNA product r.[4539_4540ins(30),4467_4539del] and the protein product p.[Arg1513_Arg1514ins10,Cys1490Glufs*12].²⁷ RT-PCR analysis with primers located in exons 38 and 44 revealed the presence of products carrying RNA defects (Fig. 2). In particular, skipping of exon 40 on its own or in combination with exon 39 was observed. To better assess the amount of aberrant

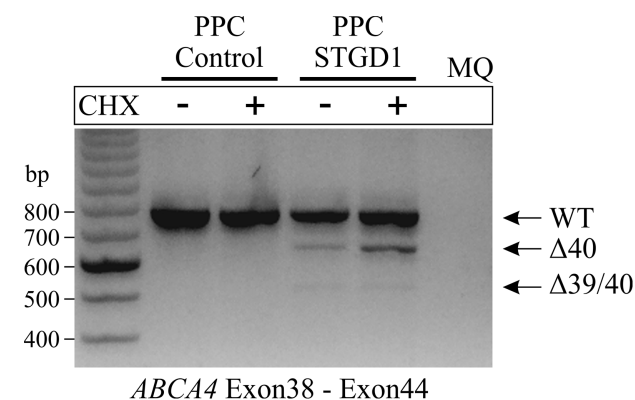


FIGURE 2. Gel image. PPCs enabled RNA analysis of the noncanonical splice site (NCSS) variant c.5714+5G>A. Control PPCs and PPCs from a patient with STGD1 were cultured without (–) or with (+) CHX that suppresses nonsense-mediated decay (NMD) owing to protein-truncating variants. RT-PCR using primers targeting exons 38 and 44 showed a 779-bp WT fragment, a 655-bp fragment corresponding with an exon 40 skipping, and a fragment of 525 bp corresponding with a combination of exon 39 and 40 skipping. The WT fragment band could be derived either from c.4539+1G>T allele, as NMD is incomplete, or from the correctly spliced product of the c.5714+5G>A allele. MQ, Milli-Q water; Δ, deletion.

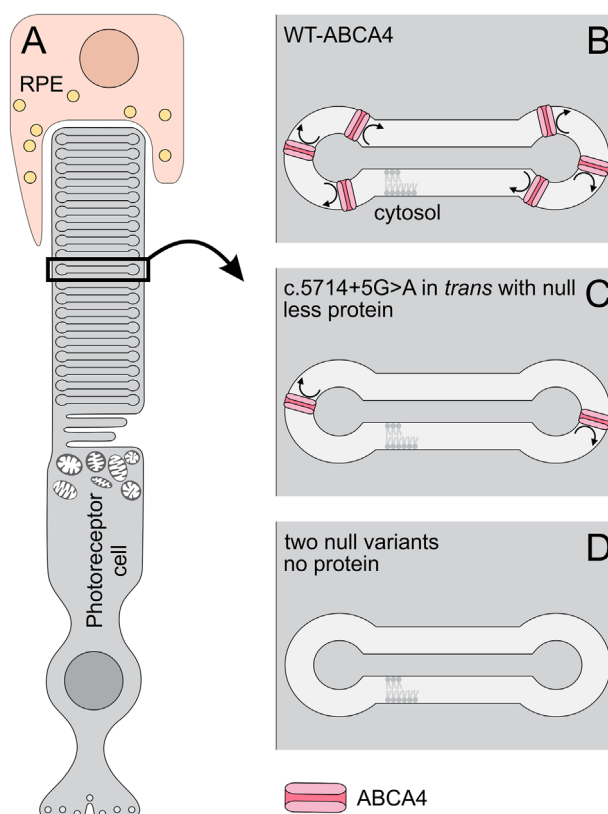


FIGURE 3. Schematic representation of the effect of the c.5714+5G>A allele. (A) RPE and photoreceptor cell with a black rectangle delineating an outer segment disc. (B) Normal number of ABCA4 transporters in a healthy person (C). Decreased number of ABCA4 transporters in a c.5714+5G>A patient. (D) Absence of ABCA4 transporters in a double null patient.

rant transcript, CHX treatment was performed to suppress the degradation of RNA products carrying protein-truncating mutations.

In the sample with no CHX treatment, the aberrantly spliced products amounted to 12.50% compared with 23.80% after CHX treatment. From 23.80% of mutant *ABCA4* mRNA treated with CHX, 20.95% of the product came from exon 39 skipping and 2.85% from a combination of exon 39 and 40 skipping, whereas 76.20% of the RT-PCR products were quantified as wild-type (WT). Because the WT fragment also contains the mRNA product of the c.4539+1G>T allele, we consider that 47.60% of mRNA from the c.5714+5G>A allele is mutant and 52.40% is WT (Fig. 3).

Clinical Analyses

The c.5714+5G>A Patients Exhibit a Milder Phenotype Than Double Null Patients. The median values for all parameters and results of statistical comparison between the two groups are shown in the Supplementary Table S4 and represented graphically in Figures 5 and 6. The c.5714+5G>A patients had a significantly later median age of onset than double null patients (17 years vs. 8 years) (Fig. 4A). At the selected time point for analysis (at the time of the latest ERG examination), the c.5714+5G>A patients were relatively older than double null patients (34 years vs. 22 years), but had a significantly milder phenotype accord-

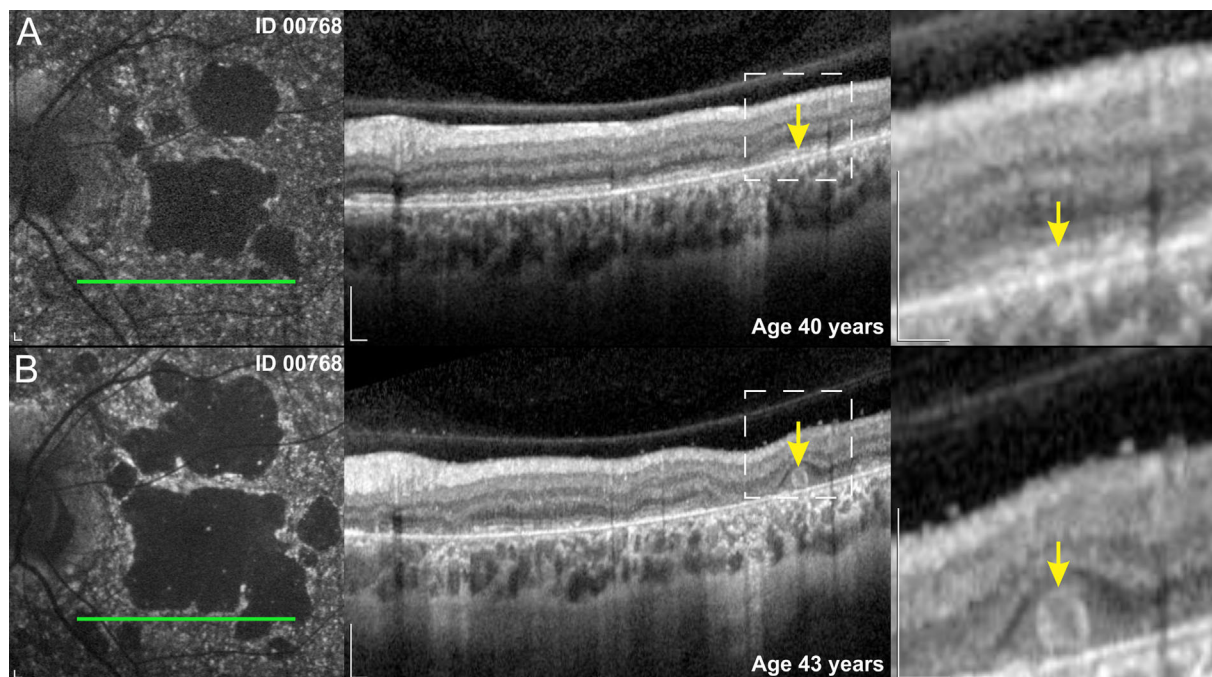


FIGURE 4. Outer nuclear tubulations. Tubulations in a c.5714+5G>A patient. Note the preserved RPE and photoreceptors layers (A), which transformed into photoreceptors grouping over the degenerating RPE in the period of 3 years (B). Scale bars, 200 μ m.

ing to all measured parameters (Figs. 5 and 6, Supplementary Table S4). ONL was measurable in all c.5714+5G>A patients and absent in all double null patients (Fig. 5C). The PERG P50 amplitude was detectable above noise level in 6 of 7 c.5714+5G>A patients (86%) and undetectable in all double null patients (Fig. 6A). The c.5714+5G>A patients had significantly higher DA 3.0 ERG a-wave amplitude (Fig. 6B), DA 0.01 ERG b-wave amplitude (Fig. 6C), LA 30 Hz ERG amplitude (Fig. 6D), and LA 3.0 ERG b-wave amplitude (Fig. 6E).

Qualitative differences were observed in the FAF and OCT images between the two groups. In c.5714+5G>A patients, the regions of decreased FAF were more often scattered and had well-defined borders, whereas in double null patients they were typically centered in the macula and had poorly defined borders (representative images in Fig. 5D and Figs. 9C, 9E, 9I, 9L). On OCT, photoreceptor tubulations were observed in c.5714+5G>A patients but not double null patients (Fig. 4 and Supplementary Fig. S5).

The c.5714+5G>A Patients Exhibit a Delayed Decline of Structural and Functional Biomarkers in Comparison With Double Null Patients. The Kaplan–Meier survival analysis predicted that the median age when 50% of the patients reached legal blindness was 34 years for c.5714+5G>A patients (95% confidence interval [CI], 25–43 years; $n = 7$) and 12 years for double null patients (95% CI, 7–17 years; $n = 7$). The difference between the groups was significant (log-rank test, $P < 0.001$) (Fig. 7).

Supplementary Table S5 shows the results of simple linear regression analysis, performed to determine the effect of age on PERG P50, ONL thickness and DDAF. In summary; in the c.5714+5G>A group, age significantly predicted the PERG P50 amplitude, ONL thickness, and DDAF area. In the double null group, age significantly predicted DDAF area. Their PERG P50 amplitude and ONL thickness were already

undetectable at that time point (at the last ERG examination), precluding statistical analysis.

The longitudinal analysis that included data from all time points showed detectable PERG50 and DDAF in double null patients and decline of all parameters with age in both patient groups (Fig. 8). The loss of RPE (DDAF area enlargement) was relatively linear in both groups, reaching extensive RPE loss with an approximate one decade difference (Fig. 8A), whereas parameters reflecting photoreceptor loss (ONL thickness and PERG P50 amplitude) decreased more rapidly in double null than c.5714+5G>A patients, reaching undetectable levels with a difference of approximately four decades (Figs. 8B and 8C).

The c.5714+5G>A Exhibit Different Ratios of RPE and Photoreceptor Damage Than Double Null Patients. The correlations between the parameter reflecting RPE damage (DDAF), and the parameters reflecting photoreceptor damage (PERG and ONL) are shown in Figure 9. Multiple linear regression comparing the ratio of RPE versus photoreceptor damage between the two genotypic groups showed that, for the same DDAF area, c.5714+5G>A patients had significantly better preserved photoreceptor structure (thicker ONL) ($B = 19.049$; 95% CI, 7.675–30.423; $\beta = 0.650$; $P = 0.003$) and photoreceptor function (higher PERG P50 amplitudes) ($B = 2.492$; 95% CI, 1.246–3.737; $\beta = 0.692$; $P = 0.001$). Two representative patient pairs with similar DDAF areas are shown in Figures 9C–9N.

Microperimetry was assessed in three representative patients from each group (Fig. 10). All three c.5714+5G>A patients exhibited good retinal sensitivity at the regions outside the central region of RPE atrophy and a shift of fixation locus near the border of the atrophy (Figs. 10A–C). All three double null patients exhibited severe loss of retinal sensitivity outside the central region of RPE atrophy and in all three cases the fixation shifted to the peripapillary region, far from the border of the atrophy (Figs. 10D–F).

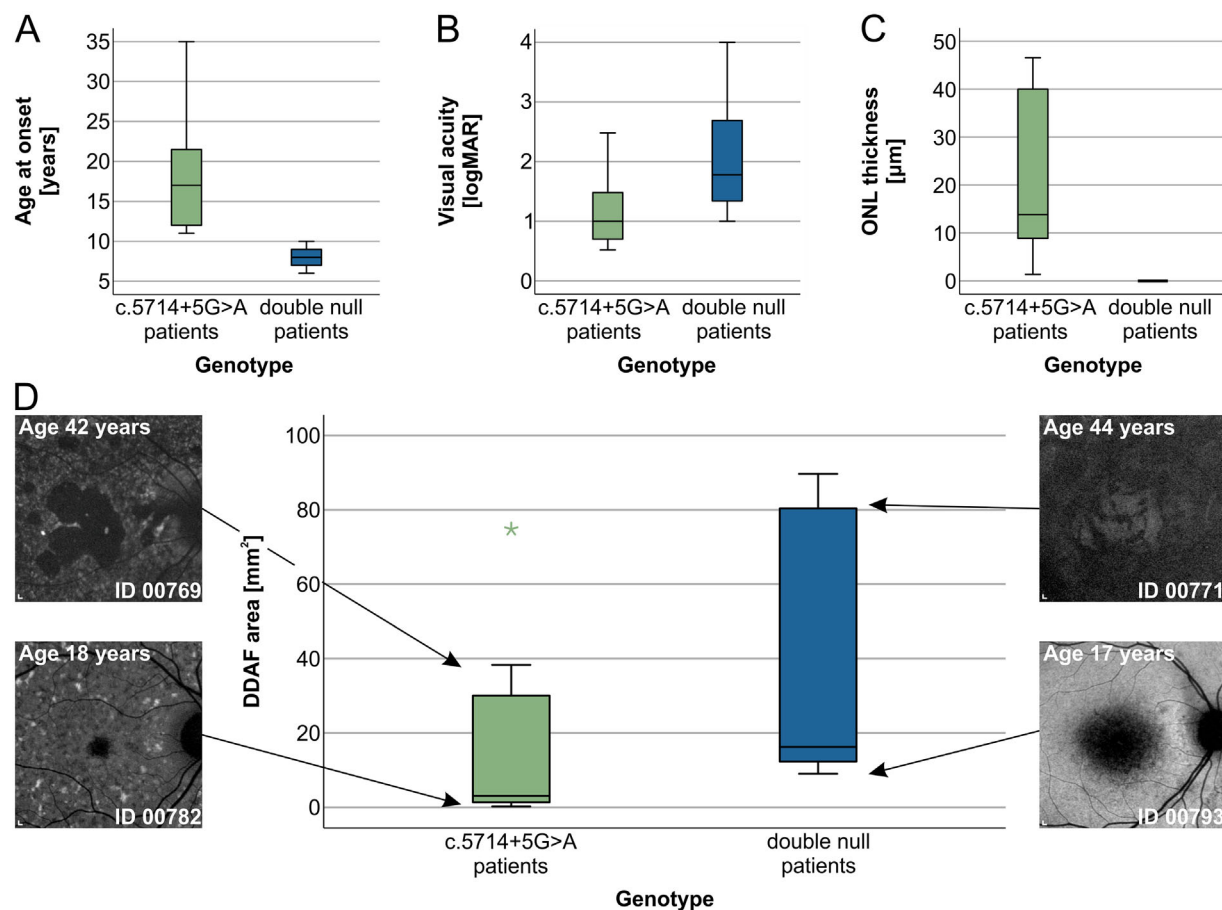


FIGURE 5. Boxplot charts showing differences between the two patient groups in the age of onset (A), VA (B), ONL thickness (C), and DDAF area (D). Horizontal lines represent median values, boxes half of the data and whiskers the remaining data except in the case of the outliers (*stars*). The c.5714+5G>A patients had significantly later age of onset, significantly better VA, thicker ONL and smaller DDAF areas than double null patients. (D) Representative FAF images of two pairs of similarly-aged patients from the two groups, shown on the left and right sides with their approximate position in the boxplot marked with arrows. Scale bars, 200 μm.

The fixation of our double null patients (Figs. 10D, 10F) shifted far from the central lesion to the peripapillary region, indicating there is an extensive loss of photoreceptor function in the maculae of these patients. In (Fig. 10E), there is a double null patient with completely eccentric fixation, indicating even more extensive loss of photoreceptor function. Note the differences between different genotypes even in patient pairs with similar degree of RPE atrophy (represented by dark areas on FAF images) (Fig. 10A vs. Fig. 10D and Fig. 10B vs. Fig. 10E).

DISCUSSION

The study combined the approaches of in vitro and clinical analyses to determine the impact of c.5714+5G>A, one of the most frequent *ABCA4* variants. The PPC assay revealed that the c.5714+5G>A allele retains approximately one-half of the WT *ABCA4* RNA and patients harboring the variant in trans with null (i.e., in isolation) exhibited signs suggestive of an RPE-first disease, contrasting the signs suggestive of photoreceptor-first disease observed in double null patients.

It was expected that disease associated with c.5714+5G>A, retaining some protein activity, would be milder than disease in double null patients. However, what is novel in this study is exploring the question whether

the disease is milder even in terms of the degree of RPE and photoreceptor damage and, if yes, in what direction. This question arises from observations of different phenotypes associated with different mild alleles. For example, the phenotype associated with the mild allele p.(Gly1961Glu) is characterized by a primary foveal photoreceptor damage and minimal to absent RPE involvement (flecks).^{9,44–46} In contrast, other mild alleles often result in a widespread RPE disease and, in some cases, spared foveal photoreceptors.^{9,46} Specific examinations of phenotypes associated with different mild alleles can improve understanding of *ABCA4* disease, especially when correlated with their effects on a molecular level.

Molecular Consequence of the c.5714+5G>A Variant

The mRNA from PPCs from a patient carrying variant c.5714+5G>A showed partially defective splicing, resulting in three RNA products, a normally spliced one and two truncated ones that presumably undergo nonsense-mediated decay. RT-PCR of mRNA from PPCs from a patient carrying c.4539+1G>T and c.5714+5G>A using primers in exons 38 and 44 showed a major normal product and

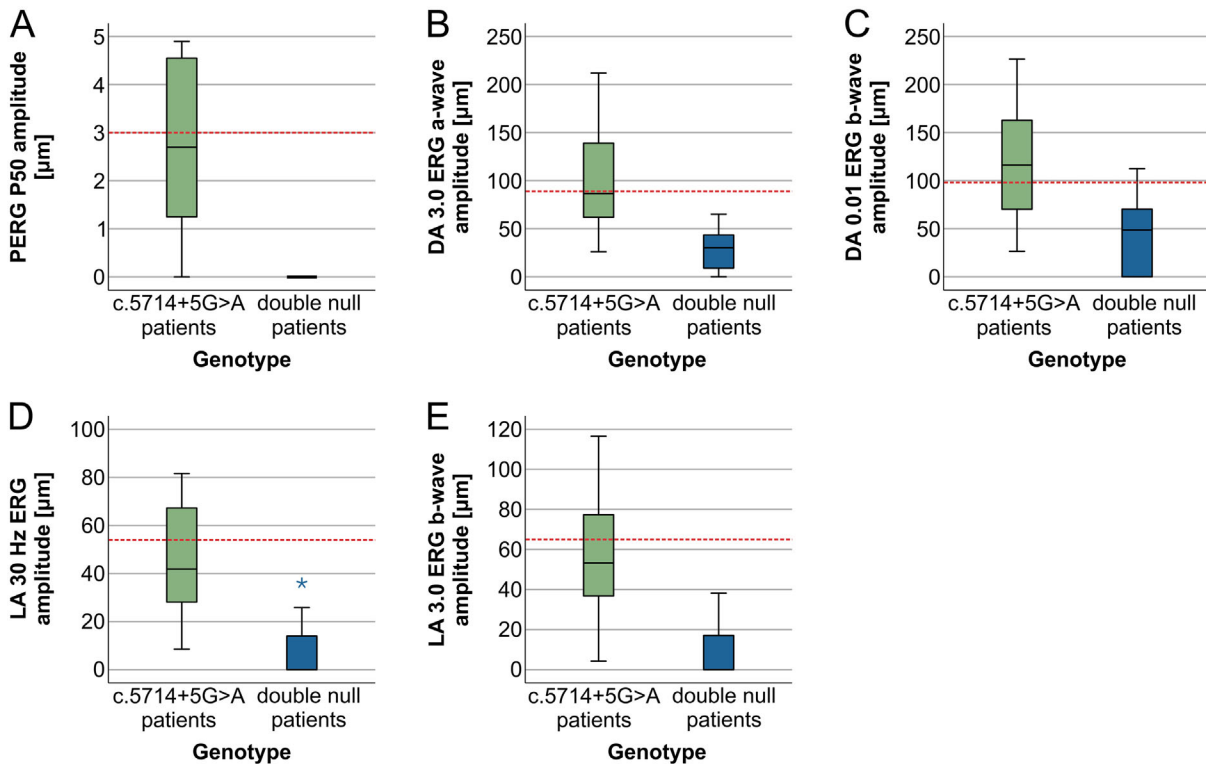


FIGURE 6. Boxplot charts showing the amplitudes of different ERG parameters in the two patient groups (A–F). Horizontal lines represent median values, boxes half of the data and whiskers the remaining data except in the case of the outliers (stars). Values were considered abnormal if they fell outside our laboratory normal range (marked with red dashed line). Note that, even though c.5714+5G>A patients were the same age or even older than double null patients, all their ERG responses were significantly better preserved, often within normal range.

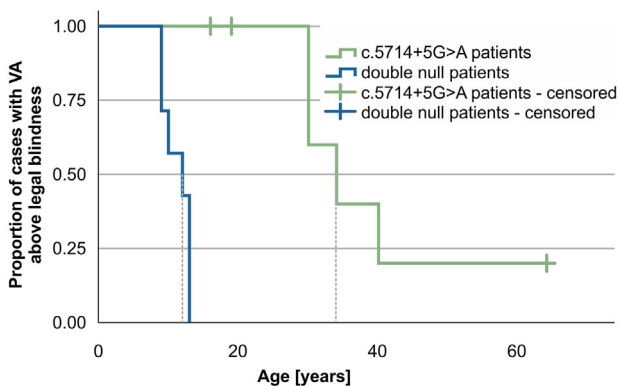


FIGURE 7. Kaplan–Meier survival analysis showing the ratio of patients reaching legal blindness (≥ 1.0 logMAR).

minor exon 40 and exon 39/40 deletion products. Quantification of the RT-PCR products showed 52.40% WT and 47.60% mutant *ABCA4* mRNA, which assumes that nonsense-mediated decay suppression is complete in CHX-treated cells. The PPC results (52.4% WT), given that these retinal-like cells better represent the in vivo situation,²⁹ partially confirm the results of the midgene-based splice assay.²⁷ These data suggest that c.5714+5G>A should be considered to behave at the boundary between mild and moderately severe.

Our results suggest that the molecular consequences of the c.5714+5G>A variant are a decrease in the abundance of normally spliced *ABCA4* mRNA owing to a partially defective splicing and, therefore, a lower quantity of the *ABCA4* transporters (Fig. 4). It remains to be seen whether there are any splicing differences between different retinal cell types, such as between photoreceptor cells and RPE cells.

Clinical Consequences of the c.5714+5G>A Variant and Implications for Disease Pathogenesis

Compared with double null patients, c.5714+5G>A patients exhibited a milder phenotype, as is expected for an allele conferring residual function.^{9,47} Although this finding was not surprising, the analysis of biomarkers representing RPE and photoreceptor damage revealed intriguing findings that suggested genotype-dependent differences in the sequence of events of disease pathogenesis. Double null patients exhibited early and severe photoreceptor loss (i.e., photoreceptor-first disease), which is in concordance with previous reports.^{13,21,48} In contrast, the clinical appearance of c.5714+5G>A patients suggested a RPE-first sequence of events, with photoreceptor loss occurring secondarily.

Three clinical observations support this premise:

- i) A lower ratio of photoreceptor versus RPE damage in c.5714+5G>A patients. Multiple regression analysis accounting for the size of RPE atrophy revealed significantly better-preserved photoreceptor structure and function in c.5714+5G>A patients. The c.5714+5G>A

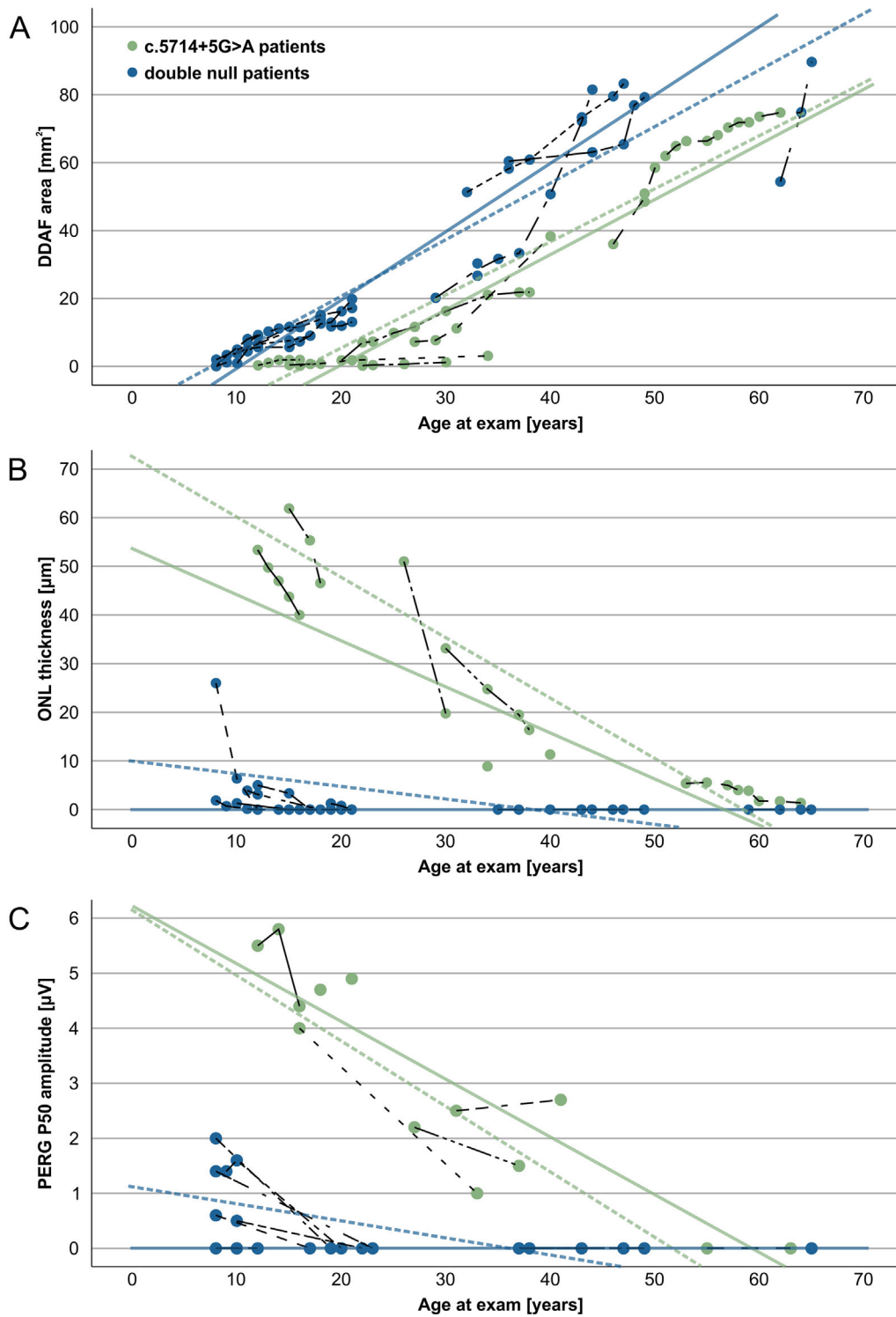


FIGURE 8. Longitudinal analysis of DDAF area (A), ONL thickness (B), and PERG P50 amplitude (C). Data points from individual patients are connected with *dashed interpolation lines*. The two *solid fit lines* are drawn using the data from exams around the last ERG testing. Dashed lines are drawn using the data from exams around the first ERG testing. The *green* represents the c.5714+5G>A patients and *blue* represents the double null patients. (A) Note a similar slope of DDAF enlargement, representing RPE loss, of the two groups, with an approximate delay of one decade in c.5714+5G>A patients (B, C). A greater time difference, of approximately four decades, was noted in parameters describing photoreceptors impairment.

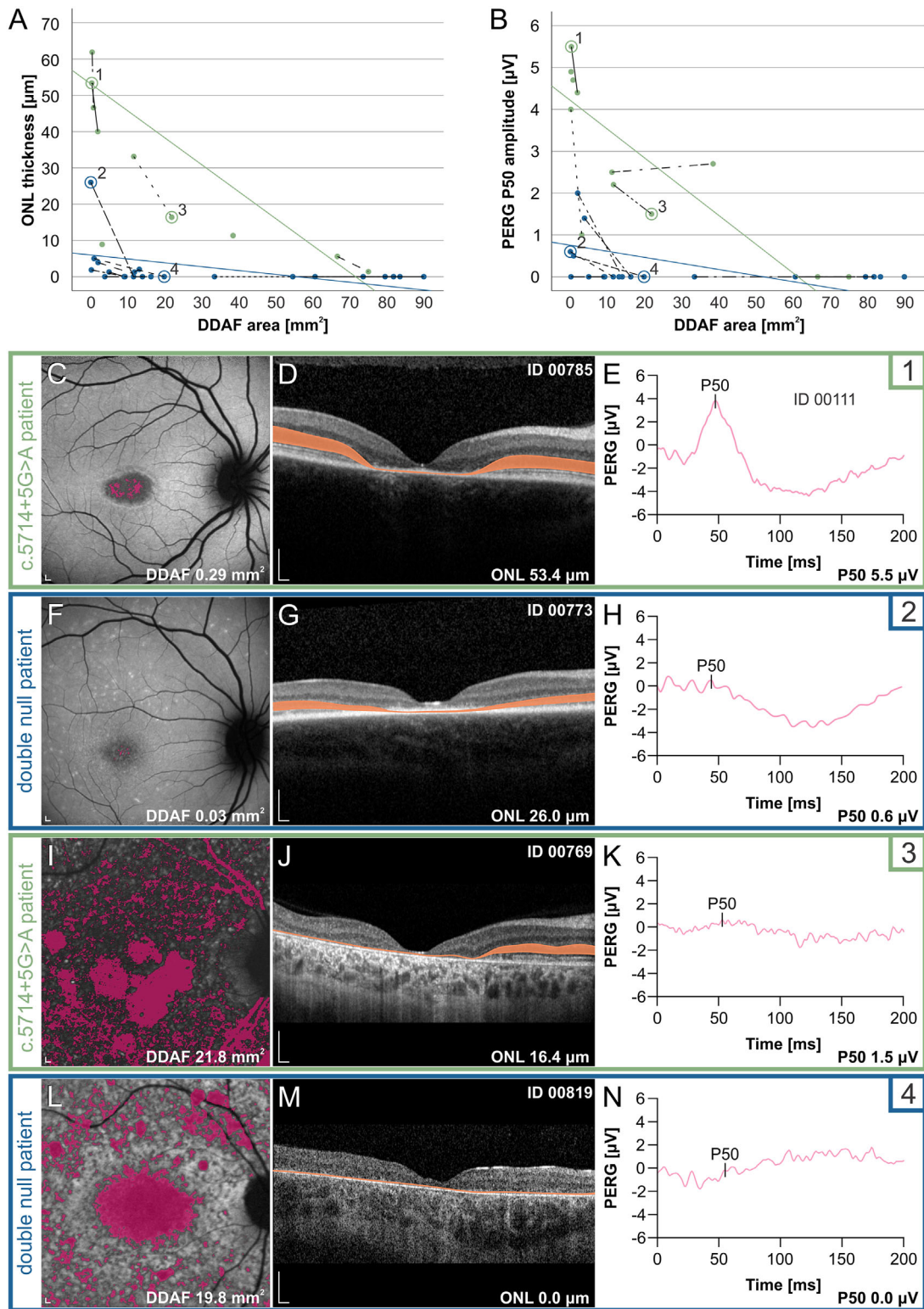


FIGURE 9. Different ratios of RPE and photoreceptor impairment in c.5714+5G>A patients (marked with *green*) and double null patients (marked with *blue*). (A) Correlation between ONL thickness and DDAF area. (B) Correlation between PERG P50 amplitude and DDAF area. Longitudinal data from the same patients are noted with *dashed lines*. Regression lines are drawn based on the first examination. (C–N) FAF, OCT scan through the fovea and PERG of representative patients with early and late stage of RPE atrophy. The individual patients are circled and marked with numbers 1 to 4 in (A) and (B). ONL is shown in orange on OCT images (D, G, J, M), and PERG P50 responses are shown in (E, H, K, N), whereas combined DDAF areas, shown in *pink*, are presented in (C, F, I, L). Note the relative preservation of ONL (A) and PERG P50 (B) of c.5714+5G>A patients across all DDAF sizes, most notable at the stage of minimal RPE atrophy, where double null patients already exhibited severe ONL and PERG P50 loss. In double null patients, a decreased ONL was observed even in the areas without notable RPE damage (RPE atrophy or extensive flecks) (F, G, L, M). Scale bars, 200 μm.

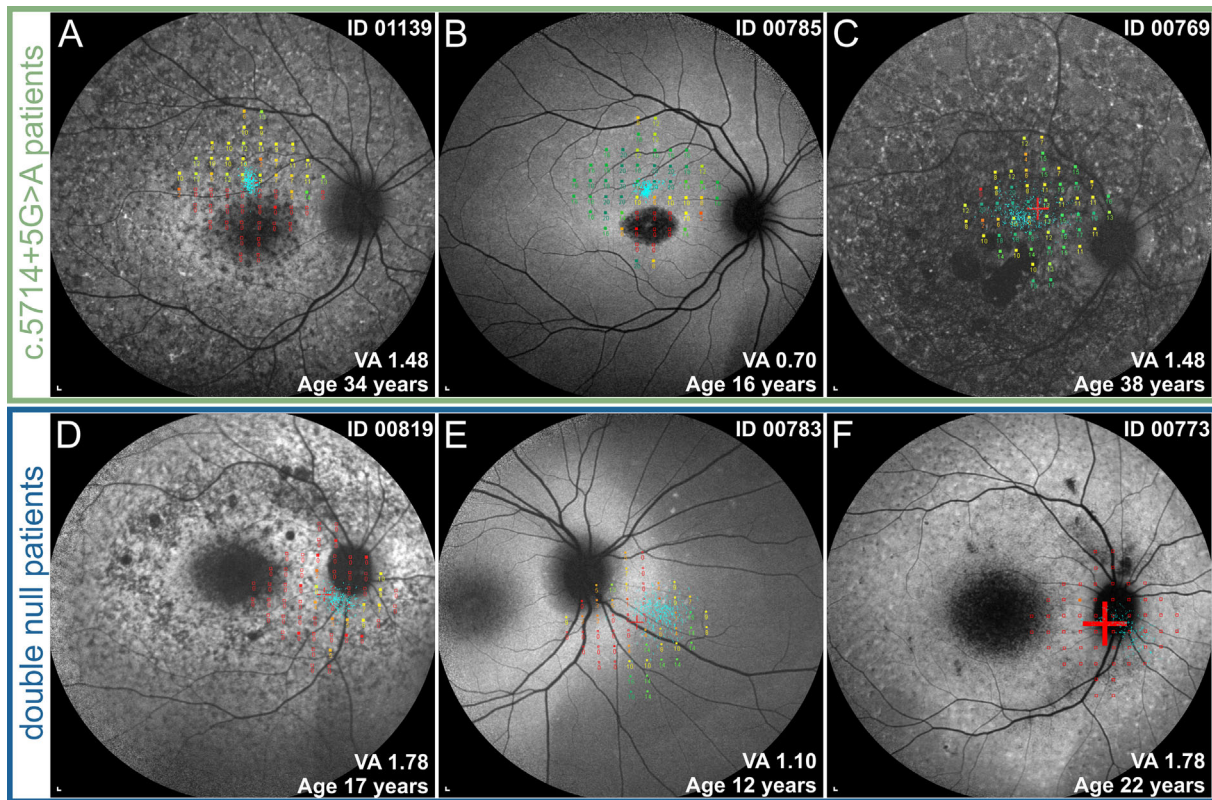


FIGURE 10. Microperimetry results superimposed over 55° FAF images in representative c.5714+5G>A patients (A–C) and double null patients (D–F). Fixation points, determining a preferred retinal locus, are marked with blue dots, and a retinal sensitivity map of 56 tested loci is projected around the fixation points. The sensitivity of tested loci is expressed as a color ranging from red (0 dB—poor sensitivity) to green (20 dB—good sensitivity). Patients with c.5714+5G>A fixated on the border of the central FAF lesion and demonstrated preserved photoreceptor function in those areas.

patients exhibited photoreceptor preservation even in the maculas with extensive RPE atrophy, whereas the double null patients exhibited severe photoreceptor impairment, even in cases with little RPE atrophy and outside of the main RPE lesion. Different ages at onset and, with that, different disease stages, are unlikely a major factor affecting the observed differences in photoreceptor preservation because differences were evident even in patient pairs with smaller degrees of RPE loss in earlier stages of the disease (Figs. 9 and 10).

- ii) Microperimetry results. It has been previously shown that after the loss of foveal cones the preferred retinal locus of fixation shifts to the area with best photoreceptor preservation.⁴⁹ Looking at microperimetry data of patient pairs with similar stage of disease in terms of RPE damage, the preferred retinal locus of fixation of c.5714+5G>A patients located next to the border of RPE atrophy, suggesting viable photoreceptors above the preserved RPE, whereas the preferred retinal locus of fixation of double null patients is located significantly further out, indicating significant photoreceptor loss above the preserved RPE (Fig. 10).
- iii) Presence of photoreceptor tubulations in c.5714+5G>A but not double null patients. Although the RPE does not depend on the presence of photoreceptors, photoreceptors cannot survive without the RPE.⁵⁰ Although the meaning of photoreceptor tubulations is not completely understood,^{51,52} they most

likely represent a short transitional period before photoreceptor degeneration in diseases that primarily affect the RPE.^{53–55} Outer retinal tubulations have previously been described in patients with STGD1 and were thought to represent primary RPE loss with viable photoreceptors grouping over the degenerating RPE.^{16,51,56} In the present study, tubulations have been observed in c.5714+5G>A, but not double null patients (Fig. 4 and Supplementary Fig. S5).

It has been proposed that ABCA4 also localizes in the RPE⁵⁷; however, the different sequence of events observed in the two patients groups is likely not a reflection of diseases of separate cell types. The RPE-first sequence of events had been proposed previously as the main hypothesis behind ABCA4 disease pathogenesis and is thought to be caused by primary RPE apoptosis after phagocytosis of bisretinoid-laden photoreceptor outer segments, followed by secondary photoreceptor degeneration.^{7,58–61} The present study supports this hypothesis in association with the c.5714+5G>A variant. In contrast, double null patients in this and previous studies¹³ exhibited signs of severe photoreceptor loss preceding RPE loss.

The results of the in vitro analysis showing defective splicing may provide some insight into the reasons behind the RPE-first sequence of events. The latter revealed defecting splicing leaving approximately 50% of normal RNA. We propose that the presence of functional ABCA4 transporters in the photoreceptor outer segments spare the photorecep-

tors from the primary degeneration, perhaps by preventing the accumulation of toxic bisretinoids on the cone outer membranes.

Unfortunately, although the timeline and the sequence of events were different, the end result in both patient groups was a severe cone-rod dystrophy; therefore, it seems that the remaining *ABCA4* protein from one c.5714+5G>A allele is not enough to prevent panretinal degeneration. The results of this study relate to the emerging gene replacement therapy, which will act in the same way, that is, by increasing the number of *ABCA4* transporters. It is, therefore, of interest to determine the level of gene expression needed to save the retina from developing disease.

Further genotype-phenotype studies are needed to determine whether our observations are variant specific or could be extrapolated to other *ABCA4* variants that result in the decreased number of functional *ABCA4* transporters. Other noncanonical splice site variants in *ABCA4* have also been shown to result in partially defective splicing,²⁷ including c.5196+1137G>A, for which the PPC assay showed approximately 55% to 60% of the normally spliced product; however, a detailed analysis of biomarkers reflecting photoreceptor and RPE loss was not performed.⁴⁷ It is important to note that the terms RPE-first and photoreceptor-first may be oversimplified. It is more likely that there are RPE-damaging and photoreceptor-damaging processes that occur simultaneously, but at a different ratio in each patient, thus, resulting in the known variability of STGD1 disease.

Other mild alleles may result in more complex effects on disease pathways, especially those affecting protein structure, its localization, and/or function. For example, biochemical experiments suggest that p.(Gly1961Glu) alters the transretinal related activity of the *ABCA4* transporter,⁶² which may be related to its specific phenotype.^{9,44} Other variants that result in mislocalization have been proposed to add an additional toxic effect to the retina.⁶³

Classification of the c.5714+5G>A Variant

Based on RNA spliced defects observed in the transfected HEK293T cells or patient-derived PPCs, the severity assessment of variants in the *ABCA4* gene can be made. Variants that showed >30% and ≤70% correct RNA were previously classified as variants with a moderate effect,⁸ and this cohort would include c.5714+5G>A with 52.40% of correct RNA. Additional modelling studies (FPMC, personal communication) indicate that variants with a moderate effect are associated with >20 and ≤40% of the remaining *ABCA4* activity, which puts c.5714+5G>A variant in the mild category. However, it should be considered, that PPCs do not fully represent the in vivo retinal situation. In fact, the gene marker analysis (Supplementary Fig. S4) showed that the patient-derived PPCs have more rod-photoreceptor and RPE cell characteristics rather than cone-photoreceptor characteristics. Additional studies of this kind are, thus, warranted. In vitro data overall have to be interpreted with caution, because they often conflict with clinical data in *ABCA4*-associated retinopathy. For example, the p.(Gly1961Glu) variant has severely abnormal activity in functional studies,⁶² but is very mild and incompletely penetrant in genetic and clinical studies.⁴⁴⁻⁴⁶ Nevertheless, the retained normally spliced product of c.5714+5G>A is not expected to have any functional or localization abnormalities; thus, the results may be more reliable.

Study Strengths and Limitations

The study's main strengths were the use of the combined in vitro and clinical approach focused on a single *ABCA4* variant, which enabled us to provide a comprehensive overview of its impact. The PPCs provided the milieu that more closely resembled the in vivo situation and the clinical part of the study included the largest genetically homogenous group of c.5714+5G>A patients so far. Moreover, quantitative analysis of DDAF, ONL, and PERG from a very similar area of the central retina allowed a precise evaluation of RPE and photoreceptor damage in patients with different genotypes. Although clinical descriptions of c.5714+5G>A were published before, they included smaller groups of patients^{9,13,30} with compound heterozygous genotypes,³⁰ and mostly qualitative assessment of ERG, FAF, images, SD-OCT images,⁹ or limited analysis of selected parameters.¹³

The limitations of the study are mostly related to the retrospective study design and low patient numbers. Although the phenotype of each group was specific enough that we were able to show significant differences for all measured parameters, a larger cohort would substantiate and strengthen our claims. Another limitation was the limitation of the Heidelberg Spectralis software, as it does not enable segmentation through the whole 30° × 30° area; thus, quantitative measurements of the ONL was only possible in the region within the Early Treatment of Diabetic Retinopathy Study (ETDRS) retinal grid, which was used to represent the ONL damage in the macula. It would be of interest to quantify the ONL outside the ETDRS area, where FAF is more often preserved; however, this factor was outside the scope of the present study. In double null patients, the qualitative analysis of ONL outside the ETDRS area showed reduced or absent photoreceptors even in the regions with preserved FAF signal (e.g., Figs. 9F, 9G, 9L, and 9M). In contrast, in c.5714+5G>A patients, photoreceptors were mainly preserved in the regions with preserved FAF signal (e.g., Figs. 9C, 9D, 9I, and 9J). Furthermore, the degree of photoreceptor impairment outside the ETDRS grid was corroborated by functional PERG and microperimetry analysis, which covered larger parts of the macula. The third limitation was that we did not measure early signs of RPE damage, but only end-stage RPE loss, that is, the DDAF area. Hyperautofluorescence quantified using quantitative FAF method has been extensively studied by Sparrow et al.⁶⁴ as a marker of early RPE damage; however, this measurement requires a special sensor, which is not available at our institution. Another parameter, questionably decreased autofluorescence has also been proposed as a biomarker of RPE damage, representing a transition zone between the healthy retina and DDAF,⁶⁵ but is very difficult to reliably quantify on FAF images. In contrast, the DDAF area, which represents RPE loss, has been defined as the most reliable biomarker for following *ABCA4* disease progression.⁶⁵⁻⁶⁹

CONCLUSIONS

We determined the effect of variant c.5714+5G>A on splicing in patient-derived PPCs, which suggested that this is a variant with a mild to moderate impact. This finding was consistent with the clinical part of the study, showing a significantly milder phenotype in c.5714+5G>A than in double null patients. Moreover, the differences in ratios of RPE and photoreceptor damage between the two patient

groups suggested genotype-dependent disease pathogenesis. Although a complete absence of the ABCA4 transporter would likely result in a photoreceptor-first disease, the presence of a decreased number of ABCA4 transporters seemingly shifts the pathogenesis toward RPE-first disease. Additional studies with larger groups of patients need to be done to confirm our observations.

Acknowledgments

The authors thank the Radboudumc Stem Cell Technology Center (<https://www.radboudumc.nl/en/research/radboud-technology-centers/stem-cells>) for reprogramming and differentiating the patient cell lines.

Supported by a fund for Young Researchers provided by the University Medical Centre Ljubljana, Ljubljana, Slovenia; the 3-moths fellowship of Jana Sajovic in a workgroup of Frans P.M. Cremers in the Department of Human Genetics in the Radboud University Medical Center, Nijmegen, the Netherlands, was funded by European Union's Horizon 2020 research and innovation under the EJP RD COFUND-EJP N° 825575; Slovenian research agency, Ljubljana, Slovenia, ARRS J3-1750; the work of Zelia Corradi was supported by a Horizon 2020, Marie Skłodowska-Curie Innovative Training Network entitled European Training Network to Diagnose, Understand and Treat Stargardt Disease, a Frequent Inherited Blinding Disorder-StarT (813490) (Frans P.M. Cremers).

Disclosure: **J. Sajovic**, None; **A. Meglič**, None; **Z. Corradi**, None; **M. Khan**, None; **A. Maver**, None; **M.J. Vidmar**, None; **M. Hawlina**, None; **F.P.M. Cremers**, None; **A. Fakin**, None

References

- Blacharski PA. Fundus flavimaculatus. In: Newsome DA, (ed). *Retinal Dystrophies and Degenerations*. New York: Raven Press; 1988:135–159.
- Molday LL, Rabin AR, Molday RS. ABCR expression in foveal cone photoreceptors and its role in Stargardt macular dystrophy. *Nat Genet*. 2000;25(3):257–258.
- Illing M, Molday LL, Molday RS. The 220-kDa rim protein of retinal rod outer segments is a member of the ABC transporter superfamily. *J Biol Chem*. 1997;272(15):10303–10310.
- Sun H, Nathans J. Stargardt's ABCR is localized to the disc membrane of retinal rod outer segments. *Nat Genet*. 1997;17(1):15–16.
- Papermaster DS, Converse CA, Zorn M. Biosynthetic and immunochemical characterization of large protein in frog and cattle rod outer segment membranes. *Exp Eye Res*. 1976;23(2):105–115.
- Quazi F, Molday RS. ATP-binding cassette transporter ABCA4 and chemical isomerization protect photoreceptor cells from the toxic accumulation of excess 11-cis-retinal. *Proc Natl Acad Sci USA*. 2014;111(13):5024–5029.
- Molday RS, Zhong M, Quazi F. The role of the photoreceptor ABC transporter ABCA4 in lipid transport and Stargardt macular degeneration. *Biochim Biophys Acta*. 2009;1791(7):573–583.
- Cremers FPM, Lee W, Collin RWJ, Allikmets R. Clinical spectrum, genetic complexity and therapeutic approaches for retinal disease caused by ABCA4 mutations. *Prog Retin Eye Res*. 2020;79:100861.
- Fakin A, Robson AG, Chiang JP, et al. The effect on retinal structure and function of 15 specific ABCA4 mutations: a detailed examination of 82 hemizygous patients. *Invest Ophthalmol Vis Sci*. 2016;57(14):5963–5973.
- Fujinami K, Lois N, Davidson AE, et al. A longitudinal study of Stargardt disease: clinical and electrophysiologic assessment, progression, and genotype correlations. *Am J Ophthalmol*. 2013;155(6):1075–1088.e13.
- Fishman GA. Fundus flavimaculatus. A clinical classification. *Arch Ophthalmol*. 1976;94(12):2061–2067.
- Lois N, Holder GE, Bunce C, Fitzke FW, Bird AC. Phenotypic subtypes of Stargardt macular dystrophy-fundus flavimaculatus. *Arch Ophthalmol*. 2001;119(3):359–369.
- Fakin A, Robson AG, Fujinami K, et al. Phenotype and progression of retinal degeneration associated with nullizigosity of ABCA4. *Invest Ophthalmol Vis Sci*. 2016;57(11):4668–4678.
- Tanaka K, Lee W, Zernant J, et al. The rapid-onset chorioretinopathy phenotype of ABCA4 disease. *Ophthalmology*. 2018;125(1):89–99.
- Tanna P, Strauss RW, Fujinami K, Michaelides M. Stargardt disease: clinical features, molecular genetics, animal models and therapeutic options. *Br J Ophthalmol*. 2017;101(1):25–30.
- Fujinami K, Sergouniotis PI, Davidson AE, et al. Clinical and molecular analysis of Stargardt disease with preserved foveal structure and function. *Am J Ophthalmol*. 2013;156(3):487–501.e1.
- Burke TR, Tsang SH. Allelic and phenotypic heterogeneity in ABCA4 mutations. *Ophthalmic Genet*. 2011;32(3):165–74.
- van Huet RA, Bax NM, Westeneng-Van Haaften SC, et al. Foveal sparing in Stargardt disease. *Invest Ophthalmol Vis Sci*. 2014;55(11):7467–78.
- Del Pozo-Valero M, Riveiro-Alvarez R, Blanco-Kelly F, et al. Genotype-phenotype correlations in a Spanish cohort of 506 families with bi-allelic ABCA4.
- Valkenburg D, Runhart EH, Bax NM, et al. Highly variable disease courses in siblings with Stargardt disease. *Ophthalmology*. 2019;126(12):1712–1721.
- Lambertus S, van Huet RA, Bax NM, et al. Early-onset Stargardt disease: phenotypic and genotypic characteristics. *Ophthalmology*. 2015;122(2):335–344.
- Lee W, Zernant J, Su PY, Nagasaki T, Tsang SH, Allikmets R. A genotype-phenotype correlation matrix for ABCA4 disease based on long-term prognostic outcomes. *JCI insight*. 2022;7(2):e156154.
- Al-Khuzaei S, Broadgate S, Foster CR, et al. An overview of the genetics of ABCA4 retinopathies, an evolving story. *Genes (Basel)*. 2021;12(8):1241.
- Sangermano R, Garanto A, Khan M, et al. Deep-intronic ABCA4 variants explain missing heritability in Stargardt disease and allow correction of splice defects by antisense oligonucleotides. *Genet Med*. 2019;21(8):1751–1760.
- Maugeri A, van Driel MA, van de Pol DJ, et al. The 2588G->C mutation in the ABCR gene is a mild frequent founder mutation in the Western European population and allows the classification of ABCR mutations in patients with Stargardt disease. *Am J Hum Genet*. 1999;64(4):1024–1035.
- Ścieżyńska A, Soszyńska M, Komorowski M, et al. Molecular analysis of the ABCA4 gene mutations in patients with Stargardt disease using human hair follicles. *Int J Mol Sci*. 2020;21(10):3430.
- Sangermano R, Khan M, Cornelis SS, et al. ABCA4 midgenes reveal the full splice spectrum of all reported noncanonical splice site variants in Stargardt disease. *Genome Res*. 2018;28(1):100–110.
- Sangermano R, Bax NM, Bauwens M, et al. Photoreceptor progenitor mRNA analysis reveals exon skipping resulting from the ABCA4 c.5461-10T->C mutation in Stargardt disease. *Ophthalmology*. 2016;123(6):1375–1385.
- Albert S, Garanto A, Sangermano R, et al. Identification and rescue of splice defects caused by two neighboring

- deep-intronic *ABCA4* mutations underlying Stargardt disease. *Am J Hum Genet.* 2018;102(4):517–527.
30. Cremers FP, van de Pol DJ, van Driel M, et al. Autosomal recessive retinitis pigmentosa and cone-rod dystrophy caused by splice site mutations in the Stargardt's disease gene *ABCR*. *Hum Mol Genet.* 1998;7(3):355–362.
 31. Cornelis SS, Runhart EH, Bauwens M, et al. Personalized genetic counseling for Stargardt disease: offspring risk estimates based on variant severity [Supplementary Table S2]. *Am J Hum Genet.* 2022;109(3):498–507.
 32. Smaragda K, Vassiliki K, George K, et al. Mutation spectrum of the *ABCA4* gene in a Greek cohort with Stargardt disease: identification of novel mutations and evidence of three prevalent mutated alleles. *J Ophthalmol.* 2018;2018:5706142.
 33. Tracowska AM, Kocyla-Karczmarewicz B, Rafalska A, et al. Genetic spectrum of *ABCA4*-associated retinal degeneration in Poland. *Genes (Basel).* 2019;10(12):959.
 34. Riveiro-Alvarez R, Lopez-Martinez MA, Zernant J, et al. Outcome of *ABCA4* disease-associated alleles in autosomal recessive retinal dystrophies: retrospective analysis in 420 Spanish families. *Ophthalmology.* 2013;120(11):2332–2337.
 35. Fujinami K, Strauss RW, Chiang JP-W, et al. Detailed genetic characteristics of an international large cohort of patients with Stargardt disease: ProgStar study report 8. *Br J Ophthalmol* 2019;103(3):390–397.
 36. Green JS, O'Rielly DD, Pater JA, et al. The genetic architecture of Stargardt macular dystrophy (STGD1): a longitudinal 40-year study in a genetic isolate. *Eur J Hum Genet.* 2020;28(7):925–937.
 37. Neitzel H. A routine method for the establishment of permanent growing lymphoblastoid cell lines. *Hum Genet.* 1986;73(4):320–326.
 38. Koolen L, Gagliardi G, Ten Brink SCA, et al. Generation and characterization of human induced pluripotent stem cells (iPSCs) from three patients with age-related macular degeneration carrying rare variants in the *CFH* gene. *Stem Cell Res.* 2022;60:102669.
 39. Flamier A, Barabino A, Bernier G. Differentiation of human embryonic stem cells into cone photoreceptors. *Bio-protocol.* 2016;6(14):e1870, doi:10.21769/BioProtoc.1870. Available at <https://en.bio-protocol.org/en/bpdetail?id=1870&type=0>. Accessed June 13, 2023.
 40. Schindelin J, Arganda-Carreras I, Frise E, et al. Fiji: an open-source platform for biological-image analysis. *Nat Methods.* 2012;9(7):676–682.
 41. Bach M, Brigell MG, Hawlina M, et al. ISCEV standard for clinical pattern electroretinography (PERG): 2012 update. *Doc Ophthalmol.* 2013;126(1):1–7.
 42. Robson AG, Frishman LJ, Grigg J, et al. ISCEV standard for full-field clinical electroretinography (2022 update). *Doc Ophthalmol.* 2022;144(3):165–177.
 43. Khan M, Cornelis SS, Pozo-Valero MD, et al. Resolving the dark matter of *ABCA4* for 1054 Stargardt disease probands through integrated genomics and transcriptomics. *Genet Med.* 2020;22(7):1235–1246.
 44. Burke TR, Fishman GA, Zernant J, et al. Retinal phenotypes in patients homozygous for the G1961E mutation in the *ABCA4* gene. *Invest Ophthalmol Vis Sci.* 2012;53(8):4458–4467.
 45. Cella W, Greenstein VC, Zernant-Rajang J, et al. G1961E mutant allele in the Stargardt disease gene *ABCA4* causes bull's eye maculopathy. *Exp Eye Res.* 2009;89(1):16–24.
 46. Zernant J, Lee W, Collison FT, et al. Frequent hypomorphic alleles account for a significant fraction of *ABCA4* disease and distinguish it from age-related macular degeneration. *J Med Genet.* 2017;54(6):404–412.
 47. Khan M, Arno G, Fakin A, et al. Detailed phenotyping and therapeutic strategies for intronic *ABCA4* variants in Stargardt disease. *Mol Ther Nucleic Acids.* 2020;21:412–427.
 48. Georgiou M, Kane T, Tanna P, et al. Prospective cohort study of childhood-onset Stargardt disease: fundus autofluorescence imaging, progression, comparison with adult-onset disease, and disease symmetry. *Am J Ophthalmol.* 2020;211:159–175.
 49. Greenstein VC, Santos RA, Tsang SH, Smith RT, Barile GR, Seiple W. Preferred retinal locus in macular disease: characteristics and clinical implications. *Retina.* 2008;28:1234–1240.
 50. Murakami Y, Notomi S, Hisatomi T, et al. Photoreceptor cell death and rescue in retinal detachment and degenerations. *Prog Retin Eye Res.* 2013;37:114–140.
 51. Goldberg NR, Greenberg JP, Laud K, Tsang S, Freund KB. Outer retinal tubulation in degenerative retinal disorders. *Retina.* 2013;33(9):1871–1876.
 52. Arrigo A, Aragona E, Battaglia O, et al. Outer retinal tubulation formation and clinical course of advanced age-related macular degeneration. *Sci Rep.* 2021;11(1):14735.
 53. Preti RC, Govetto A, Filho RGA, et al. optical coherence tomography analysis of outer retinal tubulations: sequential evolution and pathophysiological insights. *Retina.* 2018;38(8):1518–1525.
 54. Sergouniotis PI, Davidson AE, Lenassi E, Devery SR, Moore AT, Webster AR. Retinal structure, function, and molecular pathologic features in gyrate atrophy. *Ophthalmology.* 2012;119(3):596–605.
 55. Dolz-Marco R, Litts KM, Tan ACS, Freund KB, Curcio CA. The evolution of outer retinal tubulation, a neurodegeneration and gliosis prominent in macular diseases. *Ophthalmology.* 2017;124(9):1353–1367.
 56. Razeen MM, Cooper RF, Langlo CS, et al. Correlating photoreceptor mosaic structure to clinical findings in Stargardt disease. *Transl Vis Sci Technol.* 2016;5(2):6.
 57. Lenis TL, Hu J, Ng SY, et al. Expression of *ABCA4* in the retinal pigment epithelium and its implications for Stargardt macular degeneration. *Proc Natl Acad Sci USA.* 2018;115(47):e11120–e11127.
 58. Tsybovsky Y, Molday RS, Palczewski K. The ATP-binding cassette transporter *ABCA4*: structural and functional properties and role in retinal disease. *Adv Exp Med Biol.* 2010;703:105–125.
 59. Weng J, Mata NL, Azarian SM, Tzekov RT, Birch DG, Travis GH. Insights into the function of rim protein in photoreceptors and etiology of Stargardt's disease from the phenotype in *abcr* knockout mice. *Cell.* 1999;98(1):13–23.
 60. Glazer LC, Dryja TP. Understanding the etiology of Stargardt's disease. *Ophthalmol Clin North Am.* 2002;15(1):93–100, viii.
 61. Lin B, Cai X-B, Zheng Z-L, et al. Clinical and genetic analyses reveal novel pathogenic *ABCA4* mutations in Stargardt disease families. *Sci Rep.* 2016;6:35414.
 62. Sun H, Smallwood PM, Nathans J. Biochemical defects in *ABCR* protein variants associated with human retinopathies. *Nat Genet.* 2000;26(2):242–246.
 63. Wiszniewski W, Zaremba CM, Yatsenko AN, et al. *ABCA4* mutations causing mislocalization are found frequently in patients with severe retinal dystrophies. *Hum Mol Genet.* 2005;14(19):2769–2778.
 64. Sparrow JR, Marsiglia M, Allikmets R, et al. Flecks in recessive Stargardt disease: short-wavelength autofluorescence, near-infrared autofluorescence, and optical coherence tomography. *Invest Ophthalmol Vis Sci.* 2015;56(8):5029–5039.
 65. Strauss RW, Kong X, Ho A, et al. Progression of Stargardt disease as determined by fundus autofluorescence over a 12-month period: ProgStar report no. 11. *JAMA Ophthalmol.* 2019;137(10):1134–1145.

66. Fujinami K, Lois N, Mukherjee R, et al. A longitudinal study of Stargardt disease: quantitative assessment of fundus autofluorescence, progression, and genotype correlations. *Invest Ophthalmol Vis Sci.* 2013;54(13):8181–8190.
67. Lambertus S, Lindner M, Bax NM, et al. Progression of late-onset Stargardt disease. *Invest Ophthalmol Vis Sci.* 2016;57(13):5186–5191.
68. Jauregui R, Nuzbrokh Y, Su P-Y, et al. Retinal pigment epithelium atrophy in recessive Stargardt disease as measured by short-wavelength and near-infrared autofluorescence. *Transl Vis Sci Technol.* 2021;10:3–3.
69. Cicinelli MV, Rabiolo A, Brambati M, Viganò C, Bandello F, Battaglia Parodi M. Factors influencing retinal pigment epithelium-atrophy progression rate in Stargardt disease. *Transl Vis Sci Technol.* 2020;9(7):33.